Acta Pharmaceutica Sinica B 2024;14(12):5235−5248

Chinese Pharmaceutical Association
Institute of Materia Medica, Chinese Academy of Medical Sciences

Acta Pharmaceutica Sinica B

www.elsevier.com/locate/apsb
www.sciencedirect.com

ORIGINAL ARTICLE

Identification of USP2 as a novel target to induce degradation of KRAS in myeloma cells

Yingying Wang[a,†], Youping Zhang[a,†], Hao Luo[a,d,†], Wei Wei[e,†], Wanting Liu[g], Weiwei Wang[a], Yunzhao Wu[f], Cheng Peng[b], Yanjie Ji[a], Jianfang Zhang[b], Chujiao Zhu[a], Wenhui Bai[a], Li Xia[a], Hu Lei[a], Hanzhang Xu[a], Leimiao Yin[c], Wei Weng[a], Li Yang[a], Ligen Liu[a], Aiwu Zhou[a], Yueyue Wei[b], Qi Zhu[h], Weiliang Zhu[b], Yongqing Yang[c,*], Zhijian Xu[b,*], Yingli Wu[a,*]

[a]*Hongqiao International Institute of Medicine, Shanghai Tongren Hospital/Faculty of Basic Medicine, Chemical Biology Division of Shanghai Universities E-Institutes, Key Laboratory of Cell Differentiation and Apoptosis of the Chinese Ministry of Education, Shanghai Jiao Tong University School of Medicine, Shanghai 200025, China*
[b]*State Key Laboratory of Drug Research, Drug Discovery and Design Center, Shanghai Institute of Materia Medica, Chinese Academy of Sciences, Shanghai 201203, China*
[c]*Shanghai Research Institute of Acupuncture and Meridian, Yueyang Hospital of Integrated Traditional Chinese and Western Medicine Affiliated to Shanghai University of Traditional Chinese Medicine, Shanghai 201203, China*
[d]*School of Basic Medical Sciences, Shandong Second Medical University, Weifang 261053, China*
[e]*Department of Oncology, the First Affiliated Hospital of Anhui Medical University, Hefei 230022, China*
[f]*Yusuf Hamied Department of Chemistry, University of Cambridge, Cambridge CB2 1EW, UK*
[g]*Shanghai Chest Hospital, Shanghai Jiao Tong University School of Medicine, Shanghai 200025, China*
[h]*Department of Oral and Maxillofacial-Head and Neck Oncology, Ninth People's Hospital, College of Stomatology, Shanghai Jiao Tong University School of Medicine, Shanghai 200011, China*

Received 28 March 2024; received in revised form 12 June 2024; accepted 25 July 2024

KEY WORDS

Ubiquitin-specific protease 2;
KRAS;

Abstract Inducing the degradation of KRAS represents a novel strategy to combat cancers with KRAS mutation. In this study, we identify ubiquitin-specific protease 2 (USP2) as a novel deubiquitinating enzyme of KRAS in multiple myeloma (MM). Specifically, we demonstrate that gambogic acid (GA) forms a covalent bond with the cysteine 284 residue of USP2 through an allosteric pocket, inhibiting its deubiquitinating activity. Inactivation or knockdown of USP2 leads to the degradation of KRAS,

*Corresponding authors.
E-mail addresses: wuyingli@shsmu.edu.cn (Yingli Wu), zjxu@simm.ac.cn (Zhijian Xu), yyq@shutcm.edu.cn (Yongqing Yang).
[†]These authors made equal contributions to this work.
Peer review under the responsibility of Chinese Pharmaceutical Association and Institute of Materia Medica, Chinese Academy of Medical Sciences.

https://doi.org/10.1016/j.apsb.2024.08.019

Gambogic acid;
Multiple myeloma;
Degradation;
Ubiquitination;
Allosteric pocket;
Deubiquitination

resulting in the suppression of MM cell proliferation *in vitro* and *in vivo*. Conversely, overexpressing USP2 stabilizes KRAS and partially abrogates GA-induced apoptosis in MM cells. Furthermore, elevated USP2 levels may be associated with poorer prognoses in MM patients. These findings highlight the potential of the USP2/KRAS axis as a therapeutic target in MM, suggesting that strategically inducing KRAS degradation *via* USP2 inhibition could be a promising approach for treating cancers with KRAS mutations.

1. Introduction

KRAS protein is an essential molecular switch governing cell growth. In an unstimulated cell, the KRAS proteins are predominantly populated in the inactive GDP-binding state[1-3]. Upon the stimulation of upstream growth-promoting signals, KRAS can be activated by guanine nucleotide exchange factors (GEFs) to enter the GTP-binding state and interact with their downstream target proteins, such as RAF-kinases and PI3K, which subsequently initiate downstream signaling cascades[4-6]. In contrast, mutant KRAS is constitutively active and results in uncontrolled cell growth and subsequently, carcinogenesis[7].

KRAS mutations have been implicated in various cancers, including multiple myeloma (MM), lung, pancreatic, and colon cancers[4,8,9]. Notably, in MM, KRAS is the most frequently mutated protein, identified in approximately 22% of patients[10]. Moreover, in relapsed/refractory disease, bone marrow or circulating tumor DNA sequencing revealed activating RAS mutations in up to 70%. Mutant KRAS is correlated with reduced overall survival, elevated tumor aggressiveness, and increased tumor burden in MM patients, underscoring its pivotal role as an oncoprotein in the pathogenesis and progression of MM[11-13]. Therefore, KRAS may present a promising therapeutic target for MM treatment.

The KRAS protein has long been considered an 'undruggable' protein due to the lack of deep hydrophobic pockets that allow the tight binding of inhibitory small molecules[7]. Currently, most small molecules are designed to target a frequent KRAS mutant, $KRAS^{G12C}$, by forming a covalent bond with the cysteine 12 residue[14]. Two FDA-approved $KRAS^{G12C}$ inhibitors, sotorasib and adagrasib, have demonstrated encouraging outcomes in clinical trials; however, the effectiveness of $KRAS^{G12C}$ inhibitors is limited by rapid heterogeneous patterns of resistance and MAPK signaling reactivation after treatment[15]. In addition, few molecules have been developed to target other mutants[15-17]. Hence, new strategies are required to target mutant KRAS and inhibit its aberrant activity.

Other than developing small-molecule inhibitors, a potential approach could be to promote the degradation of KRAS[18]. The cellular stability of KRAS is controlled by a balance between ubiquitination and deubiquitination[19-22]. Specifically, KRAS can be ubiquitinated by E3 ubiquitin ligases, such as β-TRCP or LZTR1, and degraded by the proteasome[23-25]. Meanwhile, the ubiquitination of KRAS can be suppressed by deubiquitinating enzymes (DUBs), which remove the polyubiquitin chains from KRAS and thereby maintain its stability. Since the E3 ubiquitin ligases of KRAS are also frequently mutated in tumors, inhibiting the activities of KRAS's DUBs might be a more viable strategy. Although two DUBs, USP18 and OUTB1, are associated with the stability of KRAS, the DUBs that directly remove ubiquitin(s) from and stabilize KRAS remain unknown[26].

Ubiquitin-specific protease 2 (USP2) is a ubiquitin-specific protease that belongs to the DUB family. USP2 has been found to deubiquitinate and stabilize a diverse group of proteins, including HDM2/p53, Cyclin D1, PER1, Cry1, FASN, LDLR, TRAF6, TBK1, and TGFBR1−TGFBR2 complex[27-32]. As a result, USP2 plays critical roles in regulating cell survival, cell cycle, circadian rhythm, cell metabolism, inflammatory response, antiviral response, and metastasis[33-35]. On top of its broad regulatory activities, USP2 is involved in the tumorigenesis of many cancers, such as glioma, testicular cancer, breast cancer, and prostate cancer[36,37]. Nevertheless, the role of USP2 in the pathogenesis of MM remains unexplored.

In the present study, we show that USP2 is a direct DUB of KRAS in MM cells. Specifically, our initial findings indicated that the cellular levels of KRAS could be reduced by (GA), a natural product extracted from gamboge (*Garcinia hanburyi*). We then discovered that GA could covalently bind to USP2 in an allosteric manner, thereby inhibiting its activity. We further revealed that the USP2 stabilizes KRAS by deubiquitination; consequently, USP2 inactivation induced by GA could lead to the destabilization of KRAS, resulting in the suppression of MM cell proliferation *in vitro* and *in vivo*. Based on these findings, we propose that targeting the USP2/KRAS axis presents a promising avenue for MM treatment.

2. Materials and methods

2.1. Cell lines, plasmid, and agents

MM.1S and RPMI 8226 cells were obtained from the American Type Culture Collection (Manassas, VA, USA). The bone marrow (BM) samples were collected from newly diagnosed MM patients at the Tongren Hospital, which is affiliated to Shanghai Jiao Tong University School of Medicine (SJTU-SM). Informed consent was obtained from all patients before the study. All manipulations were approved by the Medical Science Ethics Committee of SJTU-SM. All cells were cultured in RPMI-1640 (BasalMedia, Shanghai, China) supplemented with 10% fetal calf serum (EuroClone, Life Science Division, Milan, Italy) at 37 °C in a humidified atmosphere with 5% CO_2.

2.2. RNA isolation and real-time quantitative PCR

Total RNA was extracted from 5×10^6 cells using the TRIzol reagent (Invitrogen) following the manufacturer's instructions.

The first-strand cDNA was synthesized from 1 μg of total RNA with the RNA PCR Kit (AMV) Ver.3.0 (TaKaRa) and random primers. Then, 50 ng of total cDNA was used for real-time PCR with the SYBR Premix Ex Taq Kit (TaKaRa). The relative gene expression was analyzed by the Comparative Ct method using β-actin as endogenous control. The primers for real-time PCR are as follows: *USP2* forward 5′-ATGTCCCAGCTCTCC-3′ and *USP2* reverse 5′- AGGACGGGGTGTAGG-3′; β-Actin forward 5′-CATCCTCACCCTGAAGTACCC-3′ and β-Actin reverse 5′-A GCCTGGATAGCAACGTACATG-3′; *KRAS* forward 5′-CA GTGCAATGAGGGACCAGT-3′ and *KRAS* reverse 5′-AGCA TCCTCCACTCTCTGTCT-3′.

2.3. Cell viability assay

The Cell Counting Kit-8 (CCK-8, Dojindo, Kumamoto, Japan) assay was performed to measure cell viability according to the manufacturer's instructions. Briefly, the cells were cultured in 96-well plates, treated with drugs at the indicated concentrations, and then incubated with the CCK-8 working solution for 1−4 h at 37 °C. The resulting absorbance was detected at 450 nm in a microplate reader.

2.4. Western blotting

The cells were harvested, washed with PBS, and lysed by 2 × SDS buffer. Equal quantities of protein extract were electrophoresed using sodium dodecyl sulfate-polyacrylamide gel electrophoresis (SDS-PAGE) and transferred to nitrocellulose membranes. The membranes were blocked with 5% non-fat milk at room temperature for 1 h and incubated with primary antibodies overnight at 4 °C. The membranes were then incubated with the horseradish peroxidase (HRP)-conjugated secondary IgG antibody at room temperature for 2 h. The membranes were finally imaged using the ECL detection system (ThermoFisher, USA). The antibodies used are as follows: PARP1 (#9532, Cell Signaling Technology), p-ERK (#4370, Cell Signaling Technology), p-AKT(Ser473) (#4060, Cell Signaling Technology), β-actin (#4970, Cell Signaling Technology), USP2 (10392-1-AP, Proteintech, China), Ubiquitin (sc-8017, Santa Cruz), Vinculin (66305-1-Ig, Proteintech, China), GAPDH (60004-1-Ig, Proteintech, China), Streptavidin-HRP (s6390, Sigma−Aldrich), KRAS (12063-1-AP, Proteintech, China), GFP (50430-2-AP, Proteintech, China), FLAG (66008-4-Ig, Proteintech, China), Myc (16286-1-AP, Proteintech, China), HA (81290-1-RR, Proteintech, China).

2.5. Ub-AMC protease assay

The ubiquitin-7-amino-4-methylcoumarin (Ub-AMC) hydrolysis assays were performed at 25 °C in the assay buffer (50 mmol/L Tris/HCl, 150 mmol/L NaCl, 2 mmol/L EDTA, 2 mmol/L DTT, 1 mg/mL bovine serum albumin (Roche), pH 7.5). The recombinant USP2 (20 nmol/L) was pre-incubated with DMSO or the respective compounds (50 μmol/L) for 30 min. Then, the enzymatic reaction was initiated by adding the Ub-AMC substrate (300 nmol/L). The reaction mixture was incubated at room temperature for 1 h before the reaction was terminated by adding acetic acid (100 mmol/L). The fluorescence intensity was measured on a Synergy H4 Hybrid Microplate Reader, with a 368-nm/467-nm filter pair and a 455-nm cut-off.

2.6. Cellular thermal shift assay (CETSA)

CETSA was performed as previously described[38]. Briefly, PBS-diluted MM.1S cell suspensions were freeze-thawed three times with liquid nitrogen. The soluble fraction (lysate) was separated from the cell debris by centrifugation at 20,000 × *g* for 20 min at 4 °C. The cell lysates were equally divided into two aliquots, with one aliquot treated with DMSO and the other aliquot with GA (20 mmol/L). After 10−30 min incubation at room temperature, the respective lysates were aliquoted into 20 μL aliquots, which were heated individually at different temperatures for 3 min (Veriti thermal cycler, Applied Biosystems/Life Technologies) followed by cooling for 3 min at room temperature. The appropriate temperatures were determined by preliminary CETSA experiments. Subsequently, the heated lysates were centrifuged at 20,000 × *g* for 20 min at 4 °C to separate the soluble fractions from the precipitates. The supernatants were then subjected to SDS-PAGE and Western blot.

2.7. Purification of USP2 and UBA52

The catalytic core of *USP2*, from Asn259 to Met605, was inserted into the pET28a vector. Plasmid was transformed into *E. coli* BL21 (DE3) cells, USP2 were expressed in *E. coli* BL21(DE3) cells overnight at 37 °C. Overexpression was induced with isopropyl-β-D-thiogalactoside (0.5 mmol/L) at an OD_{600} of 0.6−0.8. Cells were harvested, and resuspended in buffer A 10 mmol/L Tris/HCl, 100 mmol/L NaCl, pH 8.0). The supernatant was separated from cell debris by centrifugation at 18,000 × *g* for 1 h at 4 °C and loaded onto a Ni-NTA column (GE Healthcare) that equilibrated with the buffer A. USP2 was gradient eluted with buffer A supplemented with 20 mmol/L to 250 mmol/L imidazole using the AKTA protein purification system. Subsequently, the eluted protein was applied to a size exclusion chromatography column (Superdex 75, HiLoad 26/60, Amersham) equilibrated with 45 mmol/L potassium phosphate (pH 6.0) and 300 mmol/L NaCl. The fractions containing USP2 were diluted 1:3 in water and concentrated using an Amicon ultracentrifugation device (10 kDa cutoff) to concentrations ranging from 10 to 50 mg/mL. The concentrated protein was flash-frozen as 20−50 μL aliquots in liquid nitrogen and stored at −80 °C before use.

Human *UBA52* was amplified from a cDNA library with the sense primer 5′-TCGCGGATCCATGCAGATCTTTGTGAAGA CCCTC-3′ and the antisense primer 5′- TCCGCTCGAGTTA TTTGACCTTCTTCTTGGGACG-3′ and cloned into Pgex-6p1 by using the restriction enzymes BamH I/Xho I.

The pGEX-6P1-UBA52 plasmid was then transfected into *E. coli* BL21(DE3), GST-UBA52 were expressed in *E. coli* BL21 (DE3) cells overnight at 16 °C. Overexpression was induced with isopropyl-β-D-thiogalactoside (0.5 mmol/L) at an OD_{600} of 0.6−0.8. Cells were harvested and resuspended in lysis buffer (10 mmol/L Tris/HCl, 140 mmol/L NaCl, 2.7 mmol/L KCl, 10 mmol/L disodium hydrogen phosphate, 1.8 mmol/L potassium dihydrogen phosphate, 0.1% NP-40, 1 mmol/L PMSF, 1 mmol/L Cocktail, pH 8.0). The supernatant was separated from cell debris by centrifugation at 18,000 × *g* for 1 h at 4 °C. The GST-tagged proteins were purified with a GSTCap 4FF column and eluted with the elution buffer (250 mmol/L Tris/HCl, 50 mmol/L reduced glutathione, 100 mmol/L NaCl, and 0.1% NP-40, pH 8.0). The eluted protein was then purified, concentrated, aliquoted, and snap-frozen using the same conditions as for USP2.

2.8. Kinetic determination of the USP2−GA interaction

The specific interaction between USP2 and biotin−GA follows the typical covalent binding scheme, during which USP2 forms an initial encounter complex, USP2:GA, which then irreversibly forms a covalently linked complex USP2−GA, as shown in Eq. (1):

$$\mathrm{USP2} + \mathrm{GA} \rightleftarrows \mathrm{USP2:GA} \rightarrow \mathrm{USP2{-}GA} \quad (1)$$

To determine the values of k_{inact}, the rate constant for USP2−GA formation at saturating [GA], and K_{i}, the apparent dissociation constant for the initial USP2: GA complex (USP2: GA), USP2 was incubated with a large excess of GA for different periods and the covalent linked USP2−GA complexes [USP2−GA] were analyzed by SDS gel and subsequent Western blot using streptavidin-HRP. The protein bands on the gels were quantified by densitometry. Scanning was performed at optimal exposure time where band intensity was proportional to the concentration of protein present. Gel photographic images were stored as GRAYSCALE pictures in the TIFF format and were processed using Quantity One software. Under the pseudo-first-order experimental conditions, the concentrations of USP2 and USP2−GA complex follows the equations below:

$$[\mathrm{USP2}]_t = [\mathrm{USP2}]_0 \cdot e^{-k_{\mathrm{obs}} \cdot t} \quad (2)$$

$$[\mathrm{USP2-GA}] = [\mathrm{USP2}]_0 - [\mathrm{USP2}]_t = [\mathrm{USP2}]_0 \cdot \left(1 - e^{-k_{\mathrm{obs}} \cdot t}\right) \quad (3)$$

Here, $[\mathrm{USP2}]_0$ is the initial concentration of USP2 at time point 0 and $[\mathrm{USP2}]_t$ represent the USP2 concentration at time point t. The reaction rate constant, k_{obs}, at different GA concentrations can be calculated by fitting the experimental data to Eq. (3). The values of k_{inact} and K_{i} were determined by fitting the k_{obs} values to Eq. (4):

$$k_{\mathrm{obs}} = k_{\mathrm{inact}} \cdot \frac{[\mathrm{GA}]}{[\mathrm{GA}] + K_{\mathrm{i}}} \quad (4)$$

2.9. Pull-down of gambogic acid-bound proteins

MM.1S cells were harvested and lysed in the RIPA buffer supplemented with protease and phosphatase inhibitors (Calbiochem, Darmstadt, Germany) with brief sonication. After centrifugation at 12,000 × *g* for 30 min, the supernatant was collected. Two equally amounts of supernatants were incubated with biotin or biotin−GA for 1 h at room temperature. The mixtures were then incubated with 100 μL of Streptavidin-beads in the RIPA buffer overnight at 4 °C. After incubation, the beads were washed three times with the RIPA buffer. The bead-bound proteins were eluted, separated by SDS-PAGE, and visualized by commassie staining. The differential bands were cut down and subjected to mass spectrometry analysis.

2.10. Tumor xenograft

Experiments were performed under the approval of the Experimental Animal Ethical Committee at Shanghai Jiao Tong University School of Medicine (SJTU-SM). MM.1S or MM.1S-cas9-sgUSP2 cells were injected subcutaneously into the flanks of 6-week-old male NOD/SCID (National Cancer Institute/ National Institutes of Health) mice, respectively. A 100 μL mixture of 1×10^7 cells with 50% growth factor reduced Matrigel (BD Biosciences) was injected into each mouse. Tumor volume was calculated using Eq. (5):

$$\text{Tumor volume} = \pi/6 \times \text{Length} \times \text{Width} \times \text{High} \quad (5)$$

Mice were sacrificed for tumor dissection three weeks after the xenograft injection.

2.11. Immunohistochemical staining

Immunohistochemical experiments were performed on formalin-fixed, paraffin-embedded, 4 μm-thick tissue sections. The sections were firstly deparaffinized and rehydrated. Then, antigen retrieval was performed on the rehydrated tissue using a retrieval solution. The sections were then quenched with 0.3% hydrogen peroxide in methanol for 30 min to block endogenous peroxidase activity and washed in TBS (pH 7.2). Subsequently, the sections were blocked with 5% normal goat serum for 20 min and incubated with primary antibodies. For proliferation studies, the sections were stained with a Ki-67-specific antibody (Dako). Apoptotic cells were detected in sections using the TUNEL staining. The bound antibody was detected by a biotin-linked anti-rabbit secondary antibody and streptavidin-conjugated HRP enzymes in conjunction with the DAB chromagen. The counterstaining was performed with hematoxylin.

2.12. Molecular docking simulations

The initial structure of USP2 was obtained from the protein data bank (PDB ID:3NHE)[39]. In the simulation system, the protein was parameterized with AMBER99SB*-ILDNP[40]) force field and solvated in a cubic box of TIP3P water extended by 10 Å. The general Amber force field (GAFF)[41] was used for the ligand. A rational number of counterions were added to neutralize the system. The LINCS algorithm[42] was used to constrain all bonds involving hydrogen atoms. The long-range electrostatic interaction was treated by particle mesh Ewald (PME)[43] with a cutoff of 12 Å. The system was first minimized using the steepest descent algorithm to remove bad contacts. Then, the system was heated to 300 K in 5 ns with a harmonic restraint (1000 kcal/(mol·nm^2)). For the umbrella sampling, 28 windows were used with a constant force of 100 kJ/(mol·nm). In each window, we performed 50 ns simulations and used the center-of-mass distance between the ligand and the Cys284 residue as a collective variable, ranging from 32 to 5 Å. The average structure from the last 10 ns of each simulation was selected for exploring USP2 conformations that have a solvent-accessible Cys284. All simulations were performed with GROMACS 5.1.4 software patched with PLUMED 2.3[44].

2.13. Molecular docking and virtual screening

To predict the binding mode between USP2 and GA, the Covalent Dock module in the Schrödinger software suite 2020 was used with default parameters for the selected USP2 conformation. The Cys284 residue was targeted *via* the Michael addition mechanism. The ligand GA was prepared by LigPrep (Schrödinger LLC, 2020) and USP2 was prepared by Protein Prepare Wizard (Schrödinger LLC, 2020). To identify novel USP2 inhibitors targeting this pocket, a structure-based virtual screening was performed from the ChemDiv database with the smina software[45,46]. The random seed was explicitly set to 0.

2.14. Statistical analysis

All the experiments were repeated for 3 to 4 times, and the data are presented as the mean ± standard deviation (SD). Student's *t*-test was used for the comparison between two groups. All data were analyzed utilizing GraphPad Prism 5.0, and $^{*}P < 0.05$, $^{**}P < 0.01$, $^{***}P < 0.001$, $^{****}P < 0.0001$ *versus* control group.

3. Results

3.1. GA induces the degradation of KRAS

We first screened a homemade compound library to identify the compounds that can reduce the level of KRAS using MM cell lines, MM.1S and RPMI 8226, both of which harbor $KRAS^{G12A}$ activating mutation. As shown in Fig. 1A and B, GA treatment could reduce the levels of KRAS in both cell lines, while the other compounds showed no similar or weak effect. Further experiments showed that GA could reduce the levels of KRAS in both cell lines in a concentration and time-dependent manner, together with the downstream effectors of KRAS, including p-ERK (MAPK pathway) and p-AKT (PI3K pathway) (Fig. 1C−F). Moreover, real-time qPCR analysis showed that GA did not change the transcriptional level of KRAS (Supporting Information Fig. S1), suggesting that GA may reduce KRAS at the post-transcriptional level.

To determine whether the decrease in KRAS protein levels resulted from proteasomal degradation, we treated the MM cells with GA in the presence or absence of the proteasome inhibitor MG132. The results indicated that GA-induced downregulation of KRAS protein was partially rescued by MG132, suggesting that the KRAS protein degradation is associated with the ubiquitin-proteasome pathway (Fig. 1G and H). Furthermore, we employed the cycloheximide (CHX) assay to evaluate the stability of KRAS upon GA treatment. As shown in Fig. 1I−L, the half-life of KRAS was significantly shortened upon GA treatment in the CHX assay in both cell lines. These data suggest that GA can induce the proteasomal degradation of KRAS, which in turn impairs the downstream signal transduction in MM cells.

3.2. Identification of USP2 as a novel target of GA

To identify the target of GA for its KRAS-reducing activity, we synthesized a biotin-labeled GA (Fig. 2A), which retained the ability to induce the degradation of KRAS in MM cells (Supporting Information Fig. S2A). The interacting proteins of biotin-GA in MM.1S cells were then pulled down, separated by SDS-PAGE, and stained with Coomassie blue (Fig. 2B). The differential bands were cut down and subjected to mass spectrometry analysis. Among the potential GA-interacting proteins (Supporting Information Table S1), HSP90 and USP2, two proteins related to protein degradation, attract our attention. HSP90 is a known GA target and as a chaperon protein, it can regulate the stability of various proteins[47,48]. However, HSP90 inhibitor STA9090 treatment cannot reduce the protein level of KRAS in MM.1S cells, indicating that KRAS is not a substrate of HSP90 (Supporting Information Fig. S3). Thus, we paid more attention to USP2, a novel interacting protein of GA. To further confirm that USP2 is a target of GA, the lysates of MM.1S and RPMI 8226 cells were incubated with biotin-GA, followed by precipitation with streptavidin-coated agarose beads and gel electrophoresis. Immunofluorescence staining with the antibody of USP2 and biotin also indicated that biotin-GA colocalized with USP2 (Fig. S2B). The precipitates were subsequently blotted with anti-USP2 antibodies. As shown in Fig. 2C, the biotin-GA probe effectively pulled down the USP2 protein in the cell lysates. The interaction between USP2 and GA was further confirmed by a competition experiment: the binding of biotin-GA to recombinant USP2 was competitively inhibited by higher concentrations of unlabeled GA (Fig. 2D). These findings collectively suggested the specific interaction between GA and USP2.

Next, we performed a Cellular Thermal Shift Assay (CETSA) to determine whether GA directly binds to USP2 in cells. CETSA is designed to detect direct ligand-protein interactions by measuring changes in the protein's thermal stability in the presence or absence of a ligand compound; specifically, the ligand-protein complex is posited to exhibit enhanced thermal stability compared with the protein alone. As shown in Fig. 2E and F, compared with DMSO treatment, GA increased the thermal stability of USP2 in MM.1S cells; meanwhile, no significant change in the thermal stability of vinculin (negative control) could be observed. Furthermore, the thermal stability of USP2 could be enhanced by GA in a dose-dependent manner at 55 °C (Fig. 2G−H). In addition to the CETSA results, the drug affinity-responsive target stability assay showed that GA could prevent the pronase-mediated digestion of USP2 in a dose-dependent manner (Supporting Information Fig. S4). These data collectively suggest that USP2 is a direct interacting protein of GA.

3.3. GA specifically inhibits the activity of USP2 in vitro

Considering that USP2 functions as a ubiquitin-specific protease, we hypothesized that the binding of GA to USP2 may inhibit its enzymatic activity. To test this hypothesis, A ubiquitin-7-amino-4-methylcoumarin (Ub-AMC) hydrolytic assay was performed as previously described[49]. As shown in Fig. 2I and J, GA inhibited the hydrolytic activity of USP2 against Ub-AMC in a concentration-dependent manner (Fig. 2I). The IC_{50} value of GA for inhibiting USP2 was determined to be 1.8 μmol/L (Fig. 2J). This result was further confirmed by an *in vitro* gel-based assay using GST-UBA52 as a substrate of deubiquitinating enzymes, in which GA inhibited the USP2-mediated cleavage of GST-UBA52 in a dose-dependent manner (IC_{50} = 2.7 μmol/L) (Supporting Information Fig. S5). UBA52 is a fusion protein consisting of ubiquitin at the N terminus and ribosomal protein L40 at the C terminus. Compared with Ub-AMC, UBA52 is a natural substrate of ubiquitination, and it can provide the actual biochemical events on the catalytic efficiency of DUBs[50].

Since USP2 belongs to the cysteine protease family, we questioned whether GA could also inhibit the enzymatic activities of other proteases, specifically cathepsin B (a cysteine protease) and cathepsin D (an aspartic protease). We measured the inhibitory effect of GA on cathepsin B and cathepsin D compared with those of their inhibitors, E64D, and pepstatin. As depicted in Supporting Information Fig. S6A and S6B, GA exerted low inhibitory effects on the activities of cathepsin B and cathepsin D, which was 23 ± 2.0% and 18.7 ± 0.98%, even at a concentration of 100 μmol/L; in contrast, E64D and pepstatin strongly inhibited the activities of cathepsin B (83.0 ± 2.2%) and cathepsin D (84.9 ± 2.46%), respectively. In addition, using GST-UBA52 as the substrate, we found that GA only exhibited weak inhibitory effects against USP7, with an IC_{50} value of 17 μmol/L (Fig. S6C). Moreover, the USP7 inhibitor, P22077 could not down-regulate

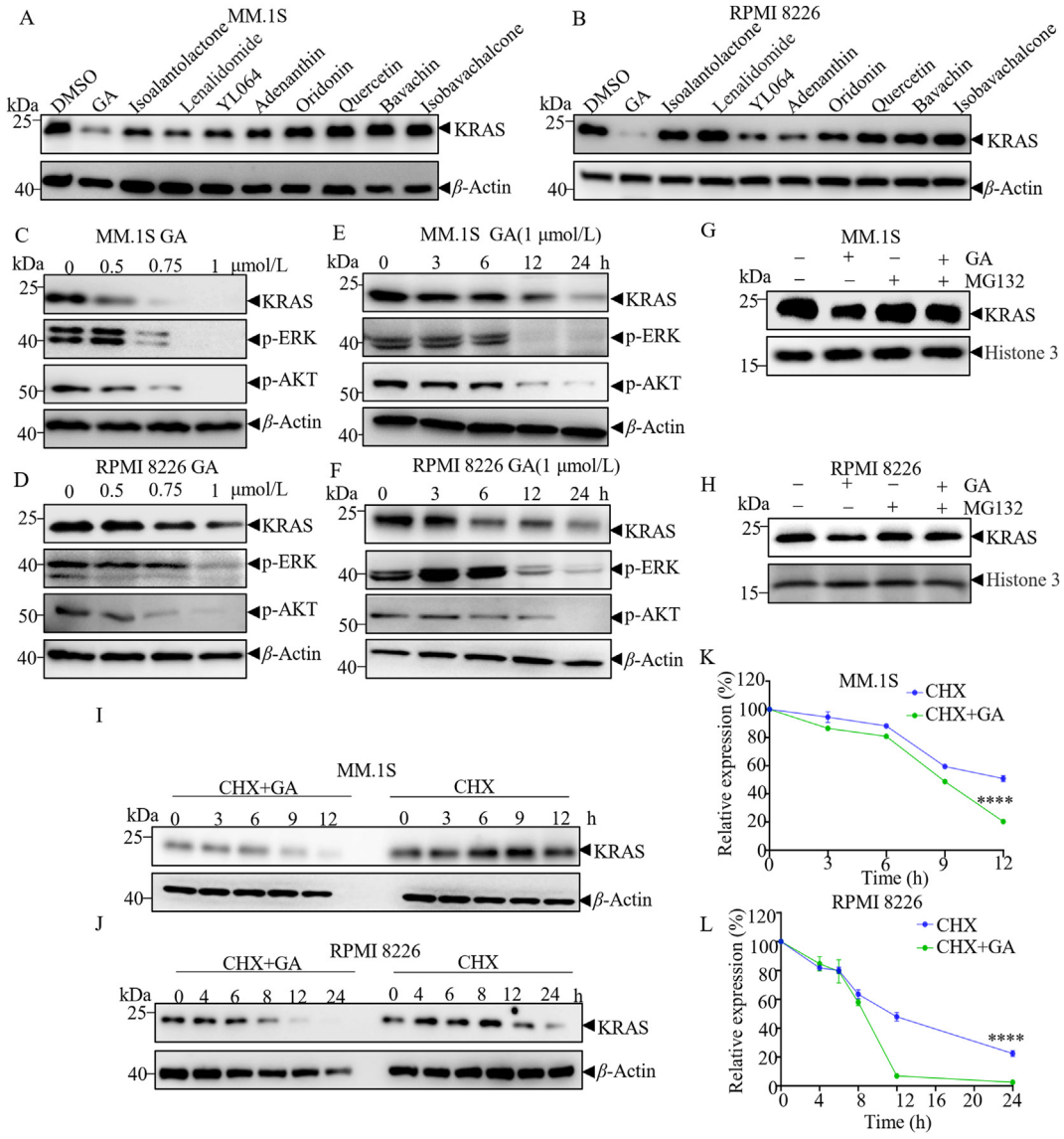

Figure 1 GA induces the degradation of KRAS. (A, B) MM.1S (A) or RPMI 8226 (B) cells were treated with the indicated compounds for 24 h. The protein levels of KRAS were then examined by Western blot. GA 1 μmol/L, isoalantolactone, lenalidomide, YL064, adenanthin, oridonin, bavachin, and isobavachalcone at 10 μmol/L, respectively. (C, D) Levels of KRAS, p-ERK, and p-AKT in MM.1S (C) and RPMI 8226 (D) cells treated with GA at different concentrations for 24 h. (E, F) Levels of KRAS, p-ERK, and p-AKT in MM.1S (E) and RPMI 8226 (F) cells treated with 1 μmol/L GA for the indicated times. (G, H) Levels of KRAS in MM.1S (G) and RPMI 8226 (H) cells treated with 1 μmol/L GA for 24 h in the presence or absence of MG132 (20 μmol/L), which was added 6 h before the cells were harvested. (I, J) Levels of KRAS in MM.1S (I) and RPMI 8226 (J) cells treated with 50 μg/mL cycloheximide (CHX) in the presence or absence of 1 μmol/L GA for the indicated times. (K, L) Relative band intensities of KRAS in (I) and (J), normalized to β-actin. Data are mean ± SD ($n = 3$), P-values were analyzed by two-way analysis of variance (ANOVA) (K, L). *$P < 0.05$, **$P < 0.01$, ***$P < 0.001$, ****$P < 0.0001$, * *versus* control group.

KRAS in MM cells but could reduce the protein level of IKZF1, one substrate of USP7, indicating KRAS is not a substrate of USP7 (Fig. S6D)[51]. Since GA is a multiple targets compound, we also tested whether GA could also target OTUB1 or USP18 and other USPs that have been reported to play a role in myeloma cells, including USP9X, USP24, USP10, USP14, USP8, USP12 and USP15[52-55], by CETSA assay. Compared to its effect on USP2, GA doesn't change the thermal stability of OTUB1, USP18, USP10, USP12, USP14, USP15, and USP8 but has a mild effect on USP9X and USP24 (Supporting Information Fig. S7A and S7B). However, WP1130, the inhibitor of USP9X and USP24, could not reduce the KRAS protein level in MM cells, indicating that USP9X and USP24 are not the DUBs for KRAS (Fig. S7C). These findings collectively suggest that GA could relatively specifically inhibit the deubiquitinating activity of USP2 *in vitro*.

3.4. Cysteine 284 is critical for the covalent binding of GA to USP2

We then investigated the mode of interaction between GA and USP2. Interestingly, preincubation of iodoacetic acid (IAA), a cysteine alkylating agent, with USP2 completely inhibited the binding of biotin-GA to USP2 (Supporting Information Fig. S8),

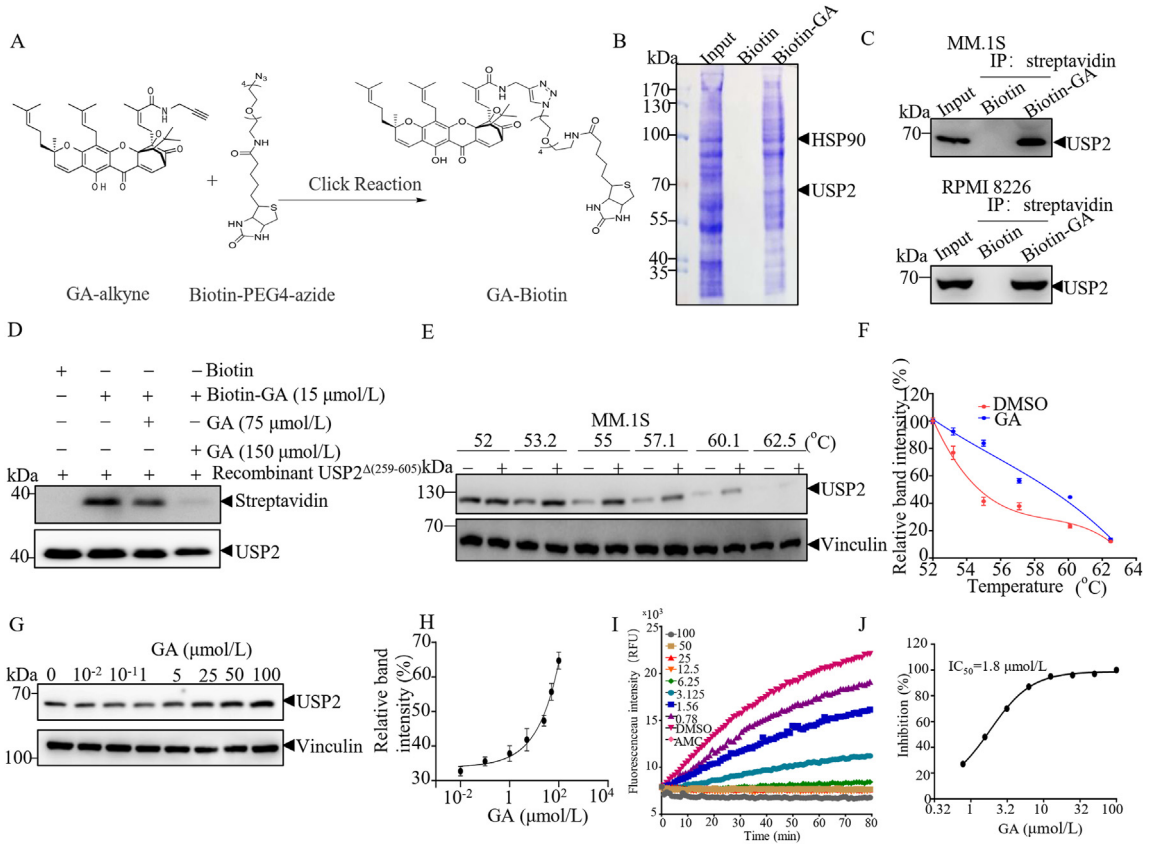

Figure 2 USP2 is a novel target of GA. (A) Synthesis of biotin−GA. (B) Coomassie brilliant blue-stained SDS-PAGE gel of precipitates pulled down by biotin−GA, 90 kDa, and 70 kDa, which were then identified by mass spectrometry to be HSP90 and USP2, respectively. (C) The precipitates pulled down by biotin−GA or biotin from MM.1S or RPMI 8226 cell lysates were examined by western blotting with anti-USP2 antibody. (D) Recombinant $USP2^{\Delta\ (259-605)}$ was incubated with biotin or biotin−GA in the absence or presence of 75 μmol/L or 150 μmol/L of unlabeled GA. The precipitates were separated by SDS-PAGE and detected by western blotting with HRP-streptavidin and anti-USP2 antibody, respectively. (E) CETSA was performed on MM.1S cells as described in materials and methods. The stabilization effect of GA on USP2 and vinculin at different temperatures. (F) Band intensities of USP2 relative to vinculin in (E). (G) Effect of different concentrations of GA on the stability of USP2 at 55 °C. (H) Relative band intensities of USP2 in (G). (I) Results of the Ub-AMC assay show that GA inhibits USP2 activity in a dose-dependent manner. (J) The IC_{50} value of GA for inhibiting USP2 was determined to be 1.8 μmol/L. Data are mean ± SD ($n = 3$), *P*-values were analyzed by two-way ANOVA (F). $^{*}P < 0.05$, $^{**}P < 0.01$, $^{***}P < 0.001$, $^{****}P < 0.0001$ *versus* control group.

suggesting that GA may covalently bind to the cysteine(s) of USP2, which is consistent with previous reports that GA can covalently bind to its targets through cysteine residues[56]. To determine the specific residue in USP2 modified by GA, we incubated the USP2 protein with GA and digested the protein with trypsin, followed by LC−MS/MS analysis. A peptide with a calculated mass of 1321.70 Da, which is 628 Da larger than the Cys284-containing peptide NSILQCLSN with a calculated mass of 693.70 Da was identified. The mass difference of 628 Da matches the molecular weight of a GA molecule. Tandem mass spectrometry of this peptide revealed that the 628 Da mass shift occurred starting from the y6 to the y11 fragment ions, indicating that the Cys284 residue was covalently modified by GA (Fig. 3A). To confirm the interaction between GA and the Cys276 residue of USP2, we constructed two mutants of USP2 by replacing Cys276 with serine (C276S) or Cys284 with serine (C284S), respectively. As shown in Fig. 3B, biotin-GA was effectively combined with the $USP2^{C276S}$ but not $USP2^{C284S}$. These data suggest that GA could specifically form a covalent bond with the Cys284 residue of USP2.

The binding kinetics of GA to USP2 were further determined by quantifying the USP2 pulled down by different concentrations of biotin-GA at different incubation time points. It can be observed from Fig. 3C that the binding of GA to USP2 was dependent on the incubation time, following the pattern of an irreversible binding mechanism. The data were then fitted to determine the observed rate constants for binding (k_{obs}) at various GA concentrations (Fig. 3D). By plotting these k_{obs} values as a function of GA concentration, a saturation curve was obtained (Fig. 3E). From this curve, the inhibition constant (K_i) and the rate of inactivation (K_{inact}) of GA to USP2 were determined to be 2.597 μmol/L and 0.03 min^{-1}, respectively. These data suggest that GA covalently binds to USP2 in a dose- and time-dependent manner.

3.5. *GA binds to USP2 through an allosteric pocket*

Intriguingly, according to the crystal data of USP2 (PDB: 2HD5), the Cys284 residue was buried inside USP2 (Supporting Information Fig. S9), suggesting that USP2 may undergo conformational changes to interact with GA. To elucidate the mode of action of GA, molecular docking simulations were performed. Firstly, umbrella sampling was employed to make Cys284 solvent accessible. Then, covalent docking was performed to

explore the binding mode of GA to USP2. As shown in Fig. 3F, molecular docking indicated that P565 and R289 are critical for forming the pocket for GA to bind to USP2. To verify this result, P565 and R289 were mutated into alanine (P565A) and leucine (R289L), respectively. These USP2 mutants were then incubated with GA and subjected to the Ub-AMC assay. The activities of the R289L (Fig. 3G and H) and P565A (Fig. 3I and J) mutants were less inhibited by GA compared with that of the WT, agreeing with the molecular docking results that P565 and R289 were critical for the GA-USP2 interaction.

We further validated the existence of this molecular pocket by employing a virtually screened USP2 inhibitor, ICU30 (Supporting Information Fig. S10A). Despite its structural dissimilarity from GA, ICU30 is also predicted to fit into this specific pocket (Fig. S10B). Using the Ub-AMC assay, we demonstrated that ICU30 could inhibit the activity of USP2 *in vitro* (Fig. S10C) with an IC_{50} of 1.2 μmol/L (Fig. S10D). Similarly, the R289L (Fig. S10E and S10F) and P565A (Fig. S10G and S10H) mutations could also abrogate the inhibitory effects of ICU30 on USP2, suggesting that ICU30 may bind to the allosteric pocket targeted by GA. Furthermore, CETSA showed that ICU30 increased the thermal stability of USP2, indicating that ICU30 interacts with USP2 in cells (Supporting Information Fig. S11A and S11B). As expected, ICU30 treatment suppressed the proliferation of MM.1S cells (Fig. S11C) and reduced the cellular protein level of KRAS in MM.1S cells (Fig. S11D) in a dose-dependent manner. To summarize, the inhibitory effect of ICU30 on USP2 not only confirmed the existence of the allosteric pocket but also highlighted its therapeutic potential in MM treatment.

3.6. *USP2 regulates the stability of KRAS*

Building on the observations that GA decreases KRAS protein levels in MM cells and inhibits USP2 activity, we hypothesized that USP2 may regulate the stability of KRAS. To test this hypothesis, we knocked out *USP2* in MM.1S and RPMI 8226 cell lines using CRISPR/Cas9. As depicted in Fig. 4A–D, the knockout of *USP2* resulted in a reduction in the KRAS protein levels (Fig. 4A and C) but not in mRNA levels (Fig. 4B and D) in both cell lines, which was similar to the effects of GA treatment.

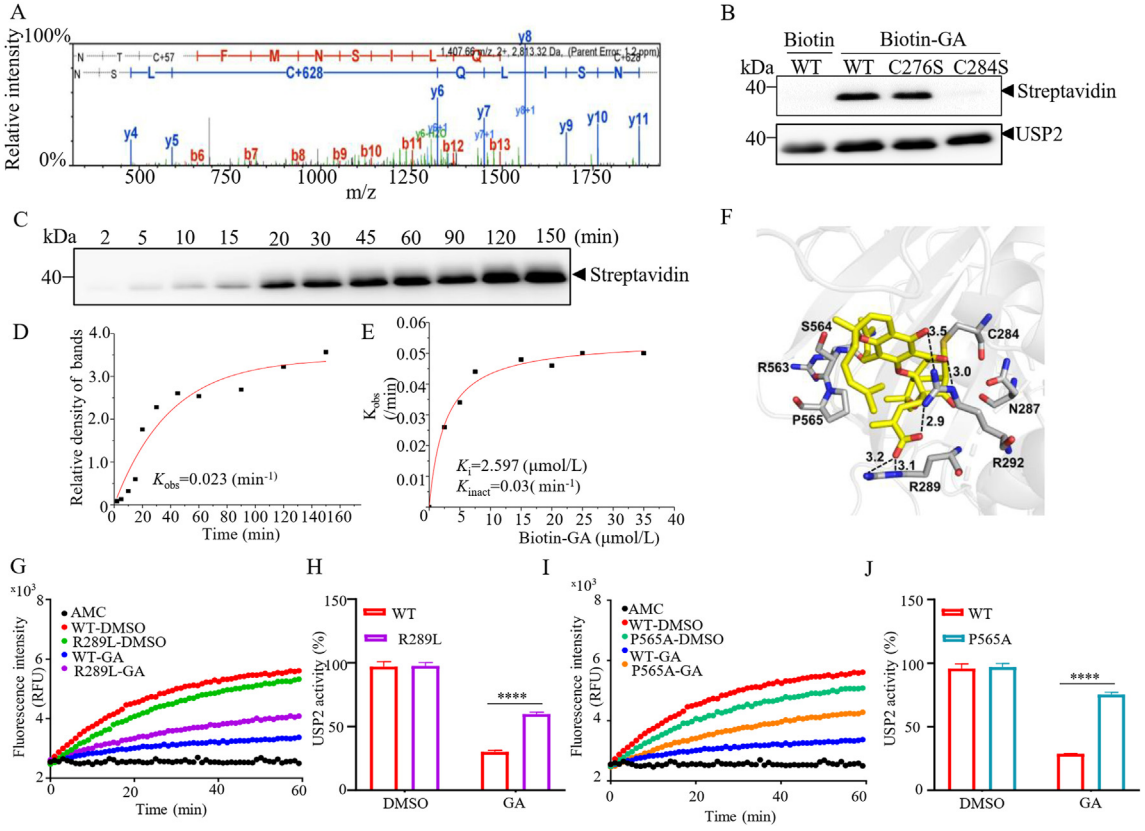

Figure 3 Cysteine 284 is critical for the binding of GA to USP2. (A) LC–MS/MS analysis. Analysis of recombinant USP2 incubated with GA for 30 min. C+ represents the Cysteine residue bound by GA. (B) Recombinant wild-type (WT) USP2 and its mutants, C276S and C284S, were incubated with biotin–GA for 30 min and blotted for biotin and USP2. (C, D) Different concentrations of biotin–GA were incubated with USP2 at various times, followed by Western blot against Biotin–GA labeled USP2. (C) The observed rate constant for binding (k_{obs}) of biotin–GA to USP2 was determined to be 0.023 min^{-1} (D). (E) By plotting k_{obs} versus biotin–GA concentration, the inhibition constant (K_i) and the rate of inactivation (K_{inact}) of GA to USP2 were determined to be 2.597 μmol/L and 0.03 min^{-1}, respectively. (F) Molecular modeling depicting the covalent binding of GA with the USP2 protein. (G, H) Ub-AMC assay comparing WT USP2 and the USP2^{R289L} mutant, indicating a reduced inhibitory effect of GA on USP2^{R289L}. (I, J) Ub-AMC assay comparing WT USP2 and the USP2^{P565A} mutant, indicating a reduced inhibitory effect of GA on USP2^{P565A}. Data are mean ± SD (n = 3), P-values were analyzed by two-way ANOVA (H, J). *P < 0.05, **P < 0.01, ***P < 0.001, ****P < 0.0001 *versus* control group.

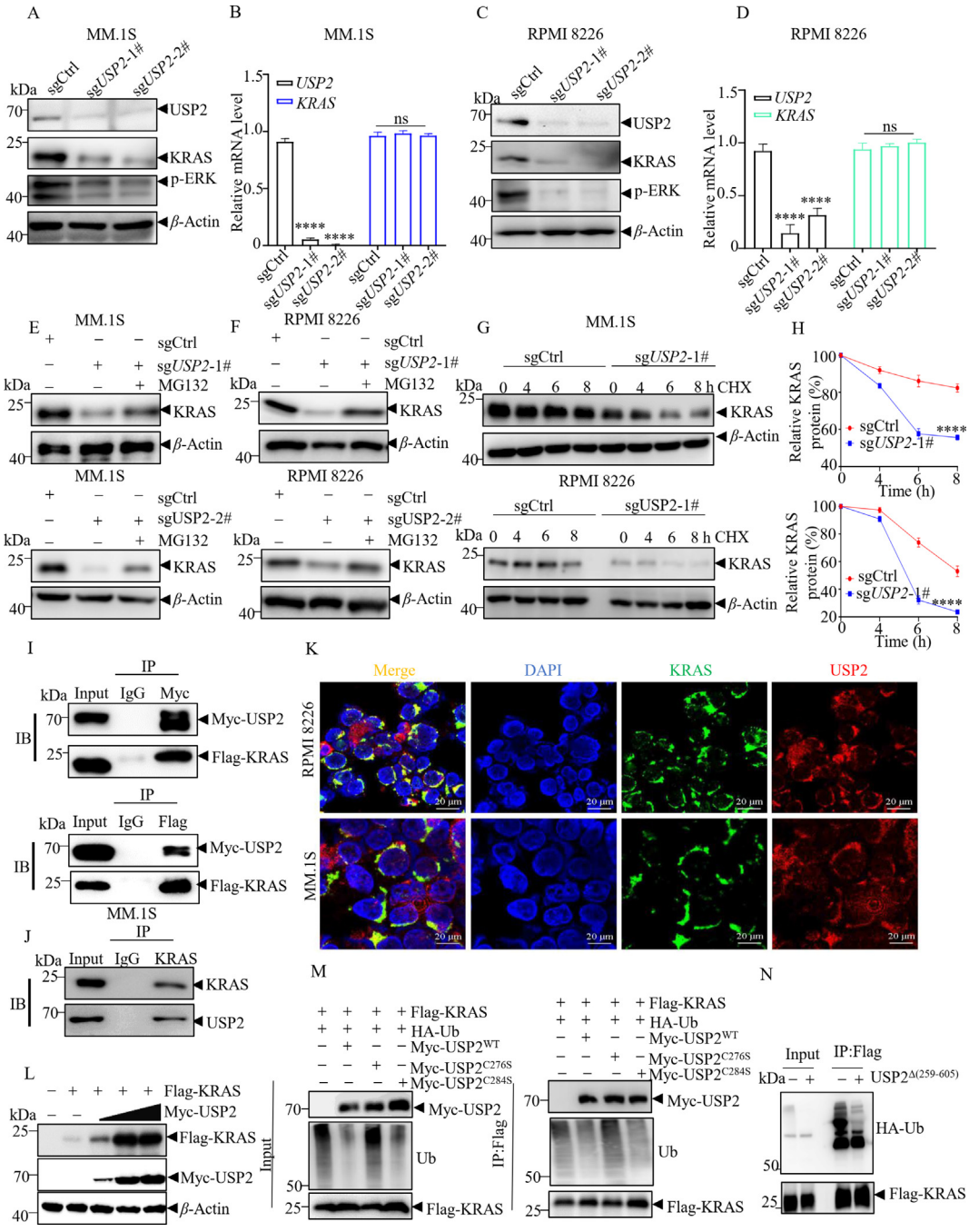

Figure 4 USP2 regulates protein level and ubiquitination of KRAS. (A−D) *USP2* was knocked out in MM.1S (A, B) or RPMI 8226 (C, D) cells by introducing *USP2*-silencing puromycin-resistant Cas9-sgRNAs. The protein levels of KRAS, p-ERK, and β-actin were detected by western blotting with the indicated antibodies (A, C). The mRNA levels of *USP2* and *KRAS* were detected by q-RT-PCR analysis (B, D). (E, F) *USP2*-knockout MM.1S (E) and RPMI 8226 (F) cells were treated with MG132 (20 μmol/L). The KRAS and β-actin levels were determined by Western blotting. (G, H) *USP2* knockout MM.1S and RPMI 8226 cells were treated with 50 μg/mL CHX for the indicated time points. The protein levels of KRAS were evaluated by Western blot (G). The KRAS band intensities were measured using ImageJ and normalized to β-actin protein levels (H). (I, J) Co-immunoprecipitation (co-IP) analysis of KRAS and USP2. Whole-cell lysates from HEK293T cells stably expressing Myc-USP2 and Flag-KRAS (I), as well as MM.1S (J) cells were immunoprecipitated and immunoblotted with antibodies against KRAS and USP2, respectively. (K) Confocal microscopic images of MM.1S and RPMI 8226 cells, show the colocalization of KRAS and USP2 in the cytoplasm. Scale bars represent 20 μm. (L) HEK293T cells stably expressing Flag-KRAS were co-transfected with an increasing dose of Myc-USP2. The protein levels of KRAS and USP2 were examined by Western blot. (M) HEK293T cells stably expressing Flag-KRAS were co-transfected with HA-Ub and Myc-USP2, Myc-USP2^{C276S} and Myc-USP2^{C284S}. The cellular extracts were immunoprecipitated with anti-Flag antibody followed by Western blot with indicated antibodies. (N) *In vitro* deubiquitination assay. HEK293T cell-derived HA-Ub-conjugated KRAS and recombinant USP2 (0.2 μg) at 37 °C for 2 h. The HA-Ub and Flag-KRAS levels were then determined by Western blot. Data are mean ± SD, *P*-values were analyzed by two-way ANOVA ($n = 3$) (B, D, H). $^{*}P < 0.05$, $^{**}P < 0.01$, $^{***}P < 0.001$, $^{****}P < 0.0001$ ns: no significance *versus* control group.

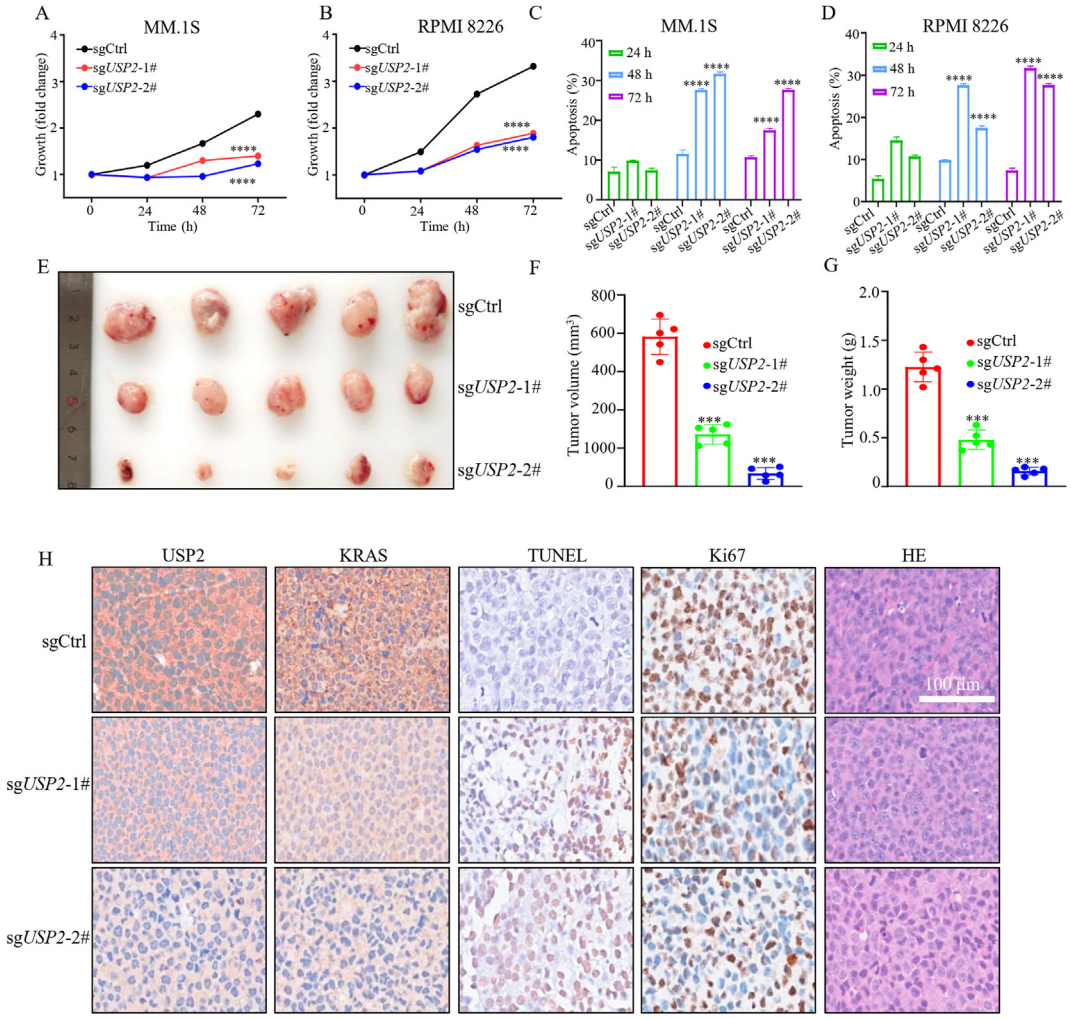

Figure 5 *USP2* depletion inhibits the proliferation of MM cells. (A−D) Effects of *USP2* knockout on the proliferation (A, B) and apoptosis (C, D) of MM.1S and RPMI 8226 cells. (E) NOD/SCID mice xenograft tumors formed by MM.1S cell line with or without *USP2* knockout. (F) Volumes of the resected tumors with or without *USP2* knockout. (G) Weights of the resected tumors with or without *USP2* knockout. (H) Immunohistochemical staining images of USP2, KRAS, TUNEL, and Ki67 of NOD/SCID mice-resected xenografts with or without *USP2* knockout. The scale bar represents 100 μm. Data are mean ± SD, *P*-values were analyzed by one-way ($n = 3$) (F, G) or two-way ($n = 5$) (C, D) ANOVA. $^{*}P < 0.05$, $^{**}P < 0.01$, $^{***}P < 0.001$, $^{****}P < 0.0001$ *versus* control group. ns: no significance.

Following the downregulation of KRAS, the levels of a downstream effector of KRAS, p-ERK were also significantly reduced (Fig. 4A and C). Moreover, *USP2* knockout-induced KRAS downregulation could be rescued by the proteasome inhibitor MG132 in both cell lines (Fig. 4E and F). *USP2* knockout also significantly shortened the half-life of KRAS (Fig. 4G and H). Taken together, these results suggest that USP2 may enhance the protein stability of KRAS.

Based on the above results, we hypothesized that USP2 may interact with and deubiquitinate KRAS. To validate this hypothesis, exogenous KRAS and USP2 were transfected into HEK293T cells. Immunoprecipitation assay showed that Flag-KRAS interacted with Myc-USP2 (Fig. 4I). Endogenous interaction of KRAS and USP2 was further verified in MM.1S cells (Fig. 4J). The immunofluorescence staining also showed that USP2 co-localized with KRAS in the cytoplasm in MM.1S and RPMI 8226 cells (Fig. 4K). Furthermore, the overexpression of USP2 increased KRAS levels in a dose-dependent manner (Fig. 4L). To determine whether USP2 deubiquitinates KRAS, $USP2^{WT}$, $USP2^{C284S}$ and its active-site mutant, $USP2^{C276S}$, were separately transfected into HEK293T cells, which were subsequently lysed and subjected to the immunoprecipitation assay. As shown in Fig. 4M, $USP2^{WT}$ and $USP2^{C284S}$, but not $USP2^{C276S}$, could remove the ubiquitin from KRAS. The deubiquitinating activity of USP2 for KRAS was further confirmed by incubating purified ubiquitinated KRAS with recombinant USP2 (Fig. 4N), which showed that ubiquitinated KRAS could be readily deubiquitinated by USP2. Taken together, these results strongly support that KRAS is a *bona fide* substrate of USP2.

3.7. *USP2 knockout inhibits the proliferation of MM cells*

Given the critical role of KRAS in the proliferation and survival of MM cells, we hypothesized that *USP2* knockout may destabilize KRAS and hence lead to MM cell proliferation inhibition. As shown in Fig. 5A and B, *USP2* knockout significantly inhibited

the proliferation of MM.1S and RPMI 8226 cell lines. *USP2* knockout also induced apoptosis in these two MM cell lines (Fig. 5C and D).

We further investigated the effect of *USP2* knockout using xenograft MM models with MM.1S cells. We found that *USP2* knockout significantly suppressed tumor growth, as indicated by the smaller tumor volumes and weights in the knockout groups compared with the control group (Fig. 5E−G). The tumor-suppressing effect of *USP2* knockout was further examined by immunohistochemistry staining of resected xenograft tumor tissue (Fig. 5H). It can be observed that *USP2* knockout resulted in cell proliferation inhibition and increased cell death, as evidenced by the decrease of Ki-67-positive and increase of TUNEL-positive cells, respectively. Notably, the immunohistochemistry staining also showed decreased levels of KRAS in the *USP2*-knockout groups but not in the control group. These data collectively suggest that the USP2 plays a critical role in the proliferation and survival of MM cells *in vitro* and *in vivo*.

3.8. GA induces the apoptosis of MM cells by targeting USP2 and destabilizing KRAS

GA has been reported to induce the apoptosis of MM cells by inhibiting the PI3K/Akt/mTOR, NF-κB, and other signaling pathways[57,58]. Consistent with these findings, GA treatment could reduce the viability and increase the apoptosis of MM.1S, and RPMI 8226 cells in a dose-dependent manner (Fig. 6A and B, Supporting Information Fig. S12). To determine whether USP2 is involved in GA-induced cytotoxic effect in MM cells, we overexpressed USP2 in RPMI 8226 cells. As shown in Fig. 6C and D, the cells overexpressing USP2 showed partial resistance to GA-induced viability reduction and KRAS degradation. Moreover, GA treatment could increase the K48-linked ubiquitination level of KRAS (Supporting Information Fig. S13). To further determine whether KRAS degradation contributes to *USP2* knockout-induced cell growth inhibition, we overexpressed KRAS^{G12C} in *USP2* knockout RPMI 8226 cells. Overexpression of KRAS^{G12C} (Fig. 6D) could partially

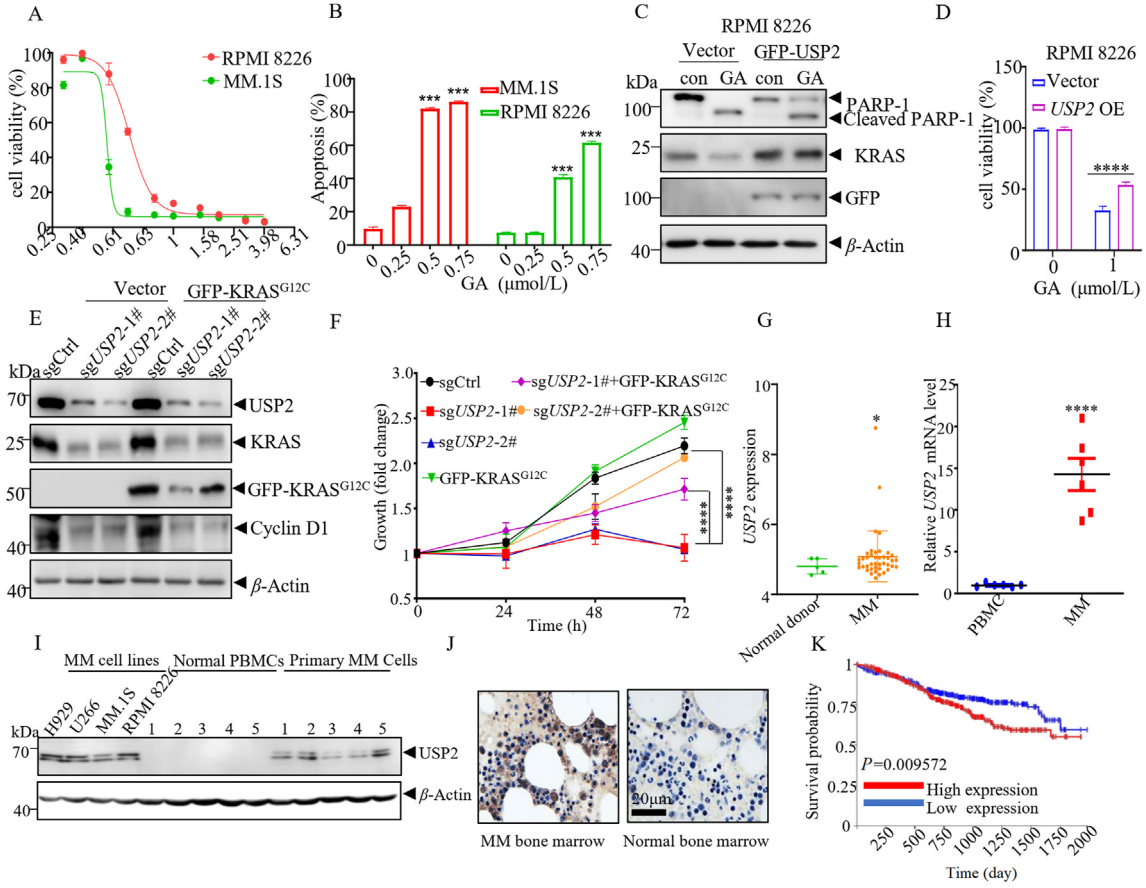

Figure 6 USP2 is a potential target in MM treatment. (A) GA treatment can reduce the cell viability of MM.1S and RPMI 8226 cell lines. (B) GA can induce apoptosis in MM.1S and RPMI 8226 cell lines ($n = 3$). (C) Overexpressing USP2 can partially abrogate GA-induced cell death in RPMI 8226 cells. (D) GA-induced cleavage PARP-1, a hallmark of apoptosis, can be partly rescued by overexpressing USP2 in RPMI 8226 cells ($n = 3$). (E) GFP-KRAS^{G12C} was overexpressed in *USP2* knockout RPMI 8226 cells and the indicated proteins were examined by Western blot. (F) The *USP2* knockout-induced cell proliferation inhibition was abrogated by KRAS^{G12C} overexpression in RPMI 8226 cells ($n = 3$). (G) Relative mRNA levels of *USP2* in normal donors ($n = 4$) and multiple myeloma cases ($n = 41$) in the GSE13591 dataset. (H) Relative mRNA levels of *USP2* in PBMC and primary myeloma cells ($n = 6$). (I) Protein levels of USP2 in MM cell lines, normal PBMCs, and primary MM cells. (J) Immunohistochemistry staining of USP2 in bone marrow biopsy samples from an MM patient (left) and a normal donor (right). The scale bar represents 20 μm. (K) Kaplan−Meier curves indicating overall survival (OS) of MM patients with low or high levels of *USP2*. Data are mean ± SD, *P*-values were analyzed by two-way ANOVA (D, F) and two-sided Student's *t*-test (G, H). $^*P < 0.05$, $^{**}P < 0.01$, $^{***}P < 0.001$, $^{****}P < 0.0001$ *versus* control group. ns: no significance.

abrogate the USP2 knockout-induced cell growth inhibition (Fig. 6E and F). These data suggest that the cytotoxicity induced by GA in MM cells is, at least in part, attributed to its targeting of USP2, which reduces the stability of KRAS.

3.9. *USP2 may be a valuable therapeutic target in MM*

Finally, we explored USP2's clinical significance in MM. Utilizing the Gene Expression Omnibus (GSE13591) database, we observed notably higher *USP2* mRNA levels in bone marrow samples from MM patients, compared with healthy donors (Fig. 6G). These results were consistent with the analysis of primary samples collected in this study (Fig. 6H). In addition, we found that the protein levels of USP2 were higher in primary myeloma cells and myeloma cell lines than in normal peripheral blood mononuclear cells (PBMCs) (Fig. 6I) and normal bone marrow biopsies (Fig. 6J). More importantly, MM patients exhibiting high *USP2* levels experienced reduced overall survival compared to those with lower *USP2* expression (Fig. 6K). These results collectively indicate a strong association between increased USP2 expression and poorer outcomes in MM, suggesting that USP2 may be a promising target for MM treatment.

4. Discussion

In this study, we reveal that USP2 is a novel deubiquitinating enzyme for KRAS. Specifically, we employed GA as a chemical probe and demonstrated that GA could covalently bind to and inhibit USP2 through an allosteric pocket. We further showed that the inhibition or knockout of USP2 could lead to the degradation of KRAS in MM cell lines, which in turn suppresses the proliferation of MM cells *in vitro* and *in vivo*. Based on these findings, we propose that USP2 is a novel target for MM therapy.

Two primary strategies to tackle cancers with KRAS mutations involve either the direct inhibition of KRAS activity or the induction of its degradation. Previous therapeutic strategies encompassed both KRAS inhibitors and proteolysis-targeting chimera (PROTAC) molecules. While small-molecule $KRAS^{G12C}$ inhibitors show promise, they are less effective against other KRAS mutations, such as the G12D mutation[20]. The efficacy of small-molecule inhibitors may also be limited due to acquired drug resistance mechanisms. On the other hand, PROTACs function by recruiting the KRAS E3 ligase, VHL, which subsequently ubiquitinates KRAS, promoting its proteasomal degradation[18]. Nevertheless, similar to the inhibitors, the warheads of PROTACs are specifically tailored for the $KRAS^{G12C}$ mutation and may also encounter challenges with drug resistance[20,59,60].

Unlike the aforementioned strategies, inhibiting the deubiquitinating enzymes of KRAS is an approach independent of KRAS mutation. The previously identified KRAS-associated DUBs include OTUB1 and USP18; however, neither of them directly deubiquitinates KRAS. Specifically, OTUB1 inhibits RAS ubiquitination independent of its catalytic activity, whereas USP18 regulates the stability of KRAS by changing its ISG15 modification and subcellular localization[19,26,60]. In the present study, we demonstrated that USP2 is a DUB that directly controls KRAS ubiquitination, as supported by the following evidence: 1) overexpression of USP2 stabilizes KRAS; 2) USP2 interacts with KRAS in cells as indicated by the immunoprecipitation and immunofluorescence assays; 3) USP2 directly removes ubiquitin from ubiquitylated KRAS, which leads to KRAS stabilization, whereas USP2 inhibition results in the proteasomal degradation of KRAS. Hence, inducing the degradation of KRAS by targeting USP2 may present a promising therapeutic strategy against cancers harboring KRAS mutations.

Identifying USP2 as a DUB of KRAS renders USP2 a promising target in MM treatment. This study highlighted that USP2 inhibition or knockdown could inhibit the proliferation of MM cells and induce MM cell apoptosis *in vitro* and *in vivo*. While these effects may be partly attributed to the degradation of KRAS, we cannot rule out other possibilities given the broad regulatory roles of USP2 in cancer. Notably, USP2 can regulate the stability of many other oncoproteins, such as MDM2, c-MYC, and Cyclin D1, which play critical roles in cancer cell survival and proliferation[32]. Moreover, we found that USP2 could also regulate the stability of NRAS and HRAS (Supporting Information Fig. S14). Therefore, further investigations are required to fully understand the roles of USP2 in MM treatment.

Intriguingly, using GA as a chemical probe, we reveal a novel allosteric pocket for inhibiting USP2. Current inhibitors of USP2, such as 6-thioguanine and ML364, predominantly target the catalytic domain of USP2[61]. Unfortunately, they have poor selectivity against USP2 because the catalytic domain is conserved among most USPs[50]. In contrast, our results indicate that GA could inhibit USP2 activity by covalently binding to the Cys284 residue, instead of the Cys276 residue within the catalytic site, of USP2. Molecular docking simulations further revealed a potential allosteric pocket for GA binding to USP2. The interaction between USP2 and GA follows a two-step mode for covalent inhibitors. That is, USP2 first forms an initial encounter complex with GA, USP2:GA, then irreversibly forms a covalently linked complex USP2-GA. The mutation of Cys284 does eliminate the covalent binding of GA to USP2, but it doesn't affect the binding of GA to the allosteric pocket. Consistent with this idea, USP2 with Cys284 mutation did not affect the deubiquitinating activity of USP2 and the thermal stability of $USP2^{Cys284S}$ could also be altered by GA (Supporting Information Fig. S15). The presence of this pocket was also validated by the discovery of ICU30, a small molecule predicted to target USP2 by binding to this pocket. While ICU30 exhibited similar effects to GA, ICU30 had low activities in inhibiting MM cell proliferation, which may be attributed to its poor water solubility. Despite this, our findings spotlight a valuable allosteric pocket on USP2 that presents potential for therapeutic exploitation.

5. Conclusions

Using GA as a chemical probe, we unveil USP2 as a direct DUB of KRAS in MM cells for the first time. In addition, we reveal an allosteric molecular pocket of the USP2 protein, which can be exploited for the design of targeted inhibitors. Our work highlights the potential of USP2 as a promising therapeutic target in MM and sheds light on the treatment of cancers with KRAS mutations.

Acknowledgements

This work was supported in part by grants from the National Natural Science Foundation of China (82170145, 82322067, 82100156, and 82374583); CAMS Innovation Fund for Medical Sciences (CIFMS): 2019-I2M-5-051; Shanghai Science and Technology Commission (20ZR1430600, 20JC1410100);

Shanghai Municipal Commission of Health and Family Planning, NO. ZY (2021-2023)-0208; Shandong Provincial Natural Science Foundation (ZR2020QH095); China Postdoctoral Science Foundation funded project (2023M742311). We thank the support from Shanghai Frontiers Science Center of Cellular Homeostasis and Human Diseases, and the Core Facility of Basic Medical Sciences, Shanghai Jiao Tong University School of Medicine.

Author contributions

Yingli Wu, Zhijian Xu and Yongqing Yang conceived and oversaw the study and writing of the manuscript. Yingying Wang, Youping Zhang, Wei Wei and Hao Luo identify the relation of KRAS and USP2, performed enzyme activity analysis, western blotting, cloning and mechanistic characterization experiments. Yingying Wang, Youping Zhang performed animal studies, cell biology and biochemistry experiments, and analysis of clinical multiple myeloma specimens. Wei Weng, Li Yang and Ligen Liu provided clinical specimens. Yingying Wang, Hao Luo, Yanjie Ji, Aiwu Zhou, Yueyue Wei purified USP2 protein and generated key functional data. Yunzhao Wu, Wanting Liu, Weiwei Wang, Cheng Peng, Jianfang Zhang, Chujiao Zhu, Wenhui Bai, Li Xia, Hu Lei, Hanzhang Xu, Leimiao Yin, Qi Zhu and Weiliang Zhu oversaw all chemistry, targeted proteomics, supported generation of mass spectrometry data and manuscript preparation. All the authors read and approved the manuscript.

Conflicts of interest

The authors declare no conflict of interest.

Appendix A. Supporting information

Supporting information to this article can be found online at https://doi.org/10.1016/j.apsb.2024.08.019.

References

1. Pylayeva-Gupta Y, Grabocka E, Bar-Sagi D. RAS oncogenes: weaving a tumorigenic web. *Nat Rev Cancer* 2011;**11**:761−74.
2. Sacco A, Federico C, Todoerti K, Ziccheddu B, Palermo V, Giacomini A, et al. Specific targeting of the KRAS mutational landscape in myeloma as a tool to unveil the elicited antitumor activity. *Blood* 2021;**138**:1705−20.
3. Cully M, Downward J. SnapShot: ras signaling. *Cell* 2008;**133:** 1292−1292.e1.
4. Thompson H. US National Cancer Institute's new Ras project targets an old foe. *Nat Med* 2013;**19**:949−50.
5. Hanahan D, Weinberg RA. Hallmarks of cancer: the next generation. *Cell* 2011;**144**:646−74.
6. Feng J, Lian Z, Xia X, Lu Y, Hu K, Zhang Y, et al. Targeting metabolic vulnerability in mitochondria conquers MEK inhibitor resistance in KRAS-mutant lung cancer. *Acta Pharm Sin B* 2023;**13**:1145−63.
7. Cox AD, Fesik SW, Kimmelman AC, Luo J, Der CJ. Drugging the undruggable RAS: mission possible?. *Nat Rev Drug Discov* 2014;**13**: 828−51.
8. Chapman MA, Lawrence MS, Keats JJ, Cibulskis K, Sougnez C, Schinzel AC, et al. Initial genome sequencing and analysis of multiple myeloma. *Nature* 2011;**471**:467−72.
9. Liu P, Wang Y, Li X. Targeting the untargetable KRAS in cancer therapy. *Acta Pharm Sin B* 2019;**9**:871−9.
10. Cook JH, Melloni GEM, Gulhan DC, Park PJ, Haigis KM. The origins and genetic interactions of KRAS mutations are allele- and tissue-specific. *Nat Commun* 2021;**12**:1808.
11. Chng WJ, Gonzalez-Paz N, Price-Troska T, Jacobus S, Rajkumar SV, Oken MM, et al. Clinical and biological significance of RAS mutations in multiple myeloma. *Leukemia* 2008;**22**:2280−4.
12. Weißbach S, Heredia-Guerrero SC, Barnsteiner S, Großhans L, Bodem J, Starz H, et al. Exon-4 mutations in KRAS affect MEK/ERK and PI3K/AKT signaling in human multiple myeloma cell lines. *Cancers (Basel)* 2020;**12**:455.
13. Shirazi F, Jones RJ, Singh RK, Zou J, Kuiatse I, Berkova Z, et al. Activating KRAS, NRAS, and BRAF mutants enhance proteasome capacity and reduce endoplasmic reticulum stress in multiple myeloma. *Proc Natl Acad Sci U S A* 2020;**117**:20004−14.
14. Zeng M, Xiong Y, Safaee N, Nowak RP, Donovan KA, Yuan CJ, et al. Exploring targeted degradation strategy for oncogenic KRAS(G12C). *Cell Chem Biol* 2020;**27**:19−31.e6.
15. Zhao Y, Murciano-Goroff YR, Xue JY, Ang A, Lucas J, Mai TT, et al. Diverse alterations associated with resistance to KRAS(G12C) inhibition. *Nature* 2021;**599**:679−83.
16. Awad MM, Liu S, Rybkin II, Arbour KC, Dilly J, Zhu VW, et al. Acquired resistance to KRAS(G12C) inhibition in cancer. *N Engl J Med* 2021;**384**:2382−93.
17. Ma S, Ji J, Tong Y, Zhu Y, Dou J, Zhang X, et al. Non-small molecule PROTACs (NSM-PROTACs): protein degradation kaleidoscope. *Acta Pharm Sin B* 2022;**12**:2990−3005.
18. Zhou C, Fan Z, Zhou Z, Li Y, Cui R, Liu C, et al. Discovery of the first-in-class agonist-based SOS1 PROTACs effective in human cancer cells harboring various KRAS mutations. *J Med Chem* 2022;**65**: 3923−42.
19. Baietti MF, Simicek M, Abbasi Asbagh L, Radaelli E, Lievens S, Crowther J, et al. OTUB1 triggers lung cancer development by inhibiting RAS monoubiquitination. *EMBO Mol Med* 2016;**8**:288−303.
20. Bond MJ, Chu L, Nalawansha DA, Li K, Crews CM. Targeted degradation of oncogenic KRAS(G12C) by VHL-recruiting PROTACs. *ACS Cent Sci* 2020;**6**:1367−75.
21. Jiang Y, Ni S, Xiao B, Jia L. Function, mechanism and drug discovery of ubiquitin and ubiquitin-like modification with multiomics profiling for cancer therapy. *Acta Pharm Sin B* 2023;**13**:4341−72.
22. Dong Y, Chen Y, Ma G, Cao H. The role of E3 ubiquitin ligases in bone homeostasis and related diseases. *Acta Pharm Sin B* 2023;**13**: 3963−87.
23. Bigenzahn JW, Collu GM, Kartnig F, Pieraks M, Vladimer GI, Heinz LX, et al. LZTR1 is a regulator of RAS ubiquitination and signaling. *Science* 2018;**362**:1171−7.
24. Abe T, Umeki I, Kanno SI, Inoue SI, Niihori T, Aoki Y. LZTR1 facilitates polyubiquitination and degradation of RAS-GTPases. *Cell Death Differ* 2020;**27**:1023−35.
25. Xu H, Zhou S, Xia H, Yu H, Tang Q, Bi F. MEK nuclear localization promotes YAP stability *via* sequestering β-TrCP in KRAS mutant cancer cells. *Cel Death Differ* 2019;**26**:2400−15.
26. Mustachio LM, Lu Y, Tafe LJ, Memoli V, Rodriguez-Canales J, Mino B, et al. Deubiquitinase USP18 loss mislocalizes and destabilizes KRAS in lung cancer. *Mol Cancer Res* 2017;**15**:905−14.
27. Magiera K, Tomala M, Kubica K, De Cesare V, Trost M, Zieba BJ, et al. Lithocholic acid hydroxyamide destabilizes Cyclin D1 and induces G_0/G_1 arrest by inhibiting deubiquitinase USP2a. *Cel Chem Biol* 2017;**24**:458−470.e18.
28. Tu Y, Xu L, Xu J, Bao Z, Tian W, Ye Y, et al. Loss of deubiquitylase USP2 triggers development of glioblastoma *via* TGF-β signaling. *Oncogene* 2022;**41**:2597−608.
29. Li Y, He X, Wang S, Shu HB, Liu Y. USP2a positively regulates TCR-induced NF-κB activation by bridging MALT1-TRAF6. *Protein Cell* 2013;**4**:62−70.
30. Nelson JK, Sorrentino V, Avagliano Trezza R, Heride C, Urbe S, Distel B, et al. The deubiquitylase USP2 regulates the LDLR pathway by counteracting the E3-ubiquitin ligase IDOL. *Circ Res* 2016;**118**: 410−9.

31. Tao BB, He H, Shi XH, Wang CL, Li WQ, Li B, et al. Up-regulation of USP2a and FASN in gliomas correlates strongly with glioma grade. *J Clin Neurosci* 2013;**20**:717−20.
32. Kitamura H, Hashimoto M. USP2-related cellular signaling and consequent pathophysiological outcomes. *Int J Mol Sci* 2021;**22**:1209.
33. Pouly D, Chenaux S, Martin V, Babis M, Koch R, Nagoshi E, et al. USP2-45 is a circadian clock output effector regulating calcium absorption at the post-translational level. *PLoS One* 2016;**11**:e0145155.
34. Yang Y, Duguay D, Fahrenkrug J, Cermakian N, Wing SS. USP2 regulates the intracellular localization of PER1 and circadian gene expression. *J Biol Rhythms* 2014;**29**:243−56.
35. Zhu HQ, Gao FH. The molecular mechanisms of regulation on USP2's alternative splicing and the significance of its products. *Int J Biol Sci* 2017;**13**:1489−96.
36. Yi J, Tavana O, Li H, Wang D, Baer RJ, Gu W. Targeting USP2 regulation of VPRBP-mediated degradation of p53 and PD-L1 for cancer therapy. *Nat Commun* 2023;**14**:1941.
37. Zhang J, Liu S, Li Q, Shi Y, Wu Y, Liu F, et al. The deubiquitylase USP2 maintains ErbB2 abundance *via* counteracting endocytic degradation and represents a therapeutic target in ErbB2-positive breast cancer. *Cel Death Differ* 2020;**27**:2710−25.
38. Berman H, Henrick K, Nakamura H. Announcing the worldwide protein data bank. *Nat Struct Biol* 2003;**10**:980.
39. Aliev AE, Kulke M, Khaneja HS, Chudasama V, Sheppard TD, Lanigan RM. Motional timescale predictions by molecular dynamics simulations: case study using proline and hydroxyproline sidechain dynamics. *Proteins* 2014;**82**:195−215.
40. Wang J, Wolf RM, Caldwell JW, Kollman PA, Case DA. Development and testing of a general amber force field. *J Comput Chem* 2004;**25**:1157−74.
41. Hess B. P-LINCS: a parallel linear constraint solver for molecular simulation. *J Chem Theor Comput* 2008;**4**:116−22.
42. Simmonett AC, Brooks BR. Analytical hessians for Ewald and particle mesh Ewald electrostatics. *J Chem Phys* 2021;**154**:104101.
43. Promoting transparency and reproducibility in enhanced molecular simulations. *Nat Methods* 2019;**16**:670−3.
44. Koes DR, Baumgartner MP, Camacho CJ. Lessons learned in empirical scoring with smina from the CSAR 2011 benchmarking exercise. *J Chem Inf Model* 2013;**53**:1893−904.
45. Liu CX, Yin QQ, Zhou HC, Wu YL, Pu JX, Xia L, et al. Adenanthin targets peroxiredoxin I and II to induce differentiation of leukemic cells. *Nat Chem Biol* 2012;**8**:486−93.
46. Cai H, Wang Y, Zhang J, Wei Z, Yan T, Feng C, et al. Discovery of novel SIRT1/2 inhibitors with effective cytotoxicity against human leukemia cells. *J Chem Inf Model* 2023;**63**:4780−90.
47. Yim KH, Prince TL, Qu S, Bai F, Jennings PA, Onuchic JN, et al. Gambogic acid identifies an isoform-specific druggable pocket in the middle domain of Hsp90β. *Proc Natl Acad Sci U S A* 2016;**113**:E4801−9.
48. Sanchez J, Carter TR, Cohen MS, Blagg BSJ. Old and new approaches to target the Hsp90 chaperone. *Curr Cancer Drug Targets* 2020;**20**:253−70.
49. Ritorto MS, Ewan R, Perez-Oliva AB, Knebel A, Buhrlage SJ, Wightman M, et al. Screening of DUB activity and specificity by MALDI-TOF mass spectrometry. *Nat Commun* 2014;**5**:4763.
50. Chen S, Liu Y, Zhou H. Advances in the development ubiquitin-specific peptidase (USP) Inhibitors. *Int J Mol Sci* 2021;**22**:4546.
51. Liu M, Zhang Y, Wu Y, Jin J, Cao Y, Fang Z, et al. IKZF1 selectively enhances homologous recombination repair by interacting with CtIP and USP7 in multiple myeloma. *Int J Biol Sci* 2022;**18**:2515−26.
52. Peterson LF, Sun H, Liu Y, Potu H, Kandarpa M, Ermann M, et al. Targeting deubiquitinase activity with a novel small-molecule inhibitor as therapy for B-cell malignancies. *Blood* 2015;**125**:3588−97.
53. Zhou L, Jiang H, Du J, Li L, Li R, Lu J, et al. USP15 inhibits multiple myeloma cell apoptosis through activating a feedback loop with the transcription factor NF-κBp65. *Exp Mol Med* 2018;**50**:1−12.
54. Li H, Roy M, Liang L, Cao W, Hu B, Li Y, et al. Deubiquitylase USP12 induces pro-survival autophagy and bortezomib resistance in multiple myeloma by stabilizing HMGB1. *Oncogene* 2022;**41**:1298−308.
55. Xu YJ, Zeng K, Ren Y, Mao CY, Ye YH, Zhu XT, et al. Inhibition of USP10 induces myeloma cell apoptosis by promoting cyclin D3 degradation. *Acta Pharmacol Sin* 2023;**44**:1920−31.
56. Yang J, Li C, Ding L, Guo Q, You Q, Jin S. Gambogic acid deactivates cytosolic and mitochondrial thioredoxins by covalent binding to the functional domain. *J Nat Prod* 2012;**75**:1108−16.
57. Suzuki E, Daniels TR, Helguera G, Penichet ML, Umezawa K, Bonavida B. Inhibition of NF-kappaB and Akt pathways by an antibody-avidin fusion protein sensitizes malignant B-cells to cisplatin-induced apoptosis. *Int J Oncol* 2010;**36**:1299−307.
58. Wang F, Zhang W, Guo L, Bao W, Jin N, Liu R, et al. Gambogic acid suppresses hypoxia-induced hypoxia-inducible factor-1α/vascular endothelial growth factor expression *via* inhibiting phosphatidylinositol 3-kinase/Akt/mammalian target protein of rapamycin pathway in multiple myeloma cells. *Cancer Sci* 2014;**105**:1063−70.
59. Wang H, Chi L, Yu F, Dai H, Gao C, Si X, et al. Annual review of KRAS inhibitors in 2022. *Eur J Med Chem* 2023;**249**:115124.
60. Yin G, Huang J, Petela J, Jiang H, Zhang Y, Gong S, et al. Targeting small GTPases: emerging grasps on previously untamable targets, pioneered by KRAS. *Signal Transduct Target Ther* 2023;**8**:212.
61. Chuang SJ, Cheng SC, Tang HC, Sun CY, Chou CY. 6-Thioguanine is a noncompetitive and slow binding inhibitor of human deubiquitinating protease USP2. *Sci Rep* 2018;**8**:3102.